

Supplement of Biogeosciences, 17, 1685–1700, 2020
<https://doi.org/10.5194/bg-17-1685-2020-supplement>
© Author(s) 2020. This work is distributed under
the Creative Commons Attribution 4.0 License.



Supplement of

Seasonal patterns of surface inorganic carbon system variables in the Gulf of Mexico inferred from a regional high-resolution ocean biogeochemical model

Fabian A. Gomez et al.

Correspondence to: Fabian A. Gomez (fabian.gomez@pucv.cl)

The copyright of individual parts of the supplement might differ from the CC BY 4.0 License.

Contents

1. Carbon module formulation
2. DIC and alkalinity in the Mississippi-Atchafalaya river system
3. Atmospheric CO₂
4. Model and observed pCO₂ patterns across the Gulf of Mexico
5. Seasonal patterns for sea surface temperature
6. Seasonal amplitude for surface aragonite saturation state and salinity
7. Seasonal patterns for surface salinity
8. Seasonal patterns for surface dissolved inorganic carbon
9. Seasonal patterns for surface total alkalinity
10. Zonal winds and carbon chemistry off northern Yucatan coast

1. Carbon module formulation

The carbon system module adds two new state variables to the GoMBio model: dissolved inorganic carbon (DIC, mmol m^{-3}) and total alkalinity (TA, mmol m^{-3}). These new state variables are described following Laurent et al. (2017) formulations. Accordingly, the time change of DIC and TA is given by the following equations:

$$\frac{\delta DIC}{\delta t} = r_{C:N} \cdot (-\mu_N + \text{excr}_{NH_4} + \text{remin}_{NH_4}) \quad (1)$$

$$\frac{\delta TA}{\delta t} = \mu_{NO_3} - \mu_{NH_4} + \text{excr}_{NH_4} + \text{remin}_{NH_4} - 2 \cdot \text{nitr} \quad (2)$$

where

$$\mu_N = \mu_{NO_3} + \mu_{NH_4}$$

$$\mu_{NO_3} = \mu_{NO_3}(\text{PS}) + \mu_{NO_3}(\text{PL})$$

$$\mu_{NH_4} = \mu_{NH_4}(\text{PS}) + \mu_{NH_4}(\text{PL})$$

$\mu_{NO_3}(\text{PS})$ is new nanophytoplankton production

$\mu_{NH_4}(\text{PS})$ is regenerated nanophytoplankton production

$\mu_{NO_3}(\text{PL})$ is new diatom production

$\mu_{NH_4}(\text{PL})$ is regenerated diatom production

$$\text{excr}_{NH_4} = \text{excr}(\text{ZS}) + \text{excr}(\text{ZL})$$

$\text{excr}(\text{ZS})$ is NH_4 excretion by microzooplankton

$\text{excr}(\text{ZL})$ is NH_4 excretion by mesozooplankton

$$\text{remin}_{NH_4} = \text{decomp}_{NH_4}(\text{DS}) + \text{decomp}_{NH_4}(\text{DL}) + \text{decomp}_{NH_4}(\text{DON})$$

$\text{decomp}(\text{DS})$ is decomposition of small detritus to NH_4

$\text{decomp}(\text{DL})$ is decomposition of large detritus to NH_4

$\text{decomp}(\text{DON})$ is decomposition of DON to NH_4

nitr: nitrification

$r_{C:N}$ is the carbon to nitrogen ratio

The formulations for $\mu_{NO_3}(\text{PS})$, $\mu_{NO_3}(\text{PL})$, $\mu_{NH_4}(\text{PS})$, $\mu_{NH_4}(\text{PL})$, $\text{excr}(\text{ZS})$, $\text{excr}(\text{ZL})$, $\text{decomp}(\text{DS})$, $\text{decomp}(\text{DL})$, $\text{decomp}(\text{DON})$, and *nitr* are described in Gomez et al. (2018) (see their Supplement Material: <https://doi.org/10.5194/bg-15-3561-2018-supplement>).

Sediment fluxes for DIC and TA are calculated according to Fennel et al. (2007) formulations, assuming instantaneous organic matter remineralization:

$$\frac{\delta DIC}{\delta t} = \frac{r_{C:N}}{\Delta z} \cdot [(w_P PL + w_{DS} DS + w_{DL} DL)] \quad (3)$$

$$\frac{\delta TA}{\delta t} = \left[(w_P PL + w_{DS} DS + w_{DL} DL) \cdot \frac{4}{16\Delta z} \right] \quad (4)$$

where

w_P is diatom sinking velocity (m s^{-1}).

w_{DS} is small detritus sinking velocity (m s^{-1})

w_{LS} is large detritus sinking velocity (m s^{-1})

PL: diatom concentration (mmol N m^{-3})

DS: small detritus concentration (mmol N m^{-3})

DL: large detritus concentration (mmol N m^{-3})

Δz : bottom layer thickness (m)

The 4/16 factor in (4) accounts for the coupled nitrification-denitrification impact on the NH_4 sediment flux.

$r_{C:N}$ is the carbon to nitrogen ratio

The air-sea CO_2 flux is described by Wanninkhof (2014) formulation:

$$F_{CO_2} = k \cdot \langle U_{10}^2 \rangle \cdot \left(\frac{Sc}{660} \right)^{-0.5} \cdot \kappa_0 \cdot (pCO_2^{water} - pCO_2^{air}) \cdot \frac{24}{100} \quad (5)$$

where

F_{CO_2} is in $\text{mmol CO}_2 \text{ m}^{-2} \text{ day}^{-1}$

$k = 0.251 (\text{cm h}^{-1})(\text{m s}^{-2})^{-2}$

U_{10} is wind speed at 10 m height (m s^{-1})

$\langle U_{10}^2 \rangle$ is the second moment of U_{10} (m s^{-1})²

Sc is the Schmidt number for CO_2 (dimensionless)

κ_0 is the solubility of CO_2 ($\text{mmol C m}^{-3} \text{ atm}^{-1}$)

pCO_2^{water} is the surface ocean $p\text{CO}_2$ (atm)

pCO_2^{air} is the atmospheric $p\text{CO}_2$ (atm)

2. DIC and alkalinity in the Mississippi-Atchafalaya river system

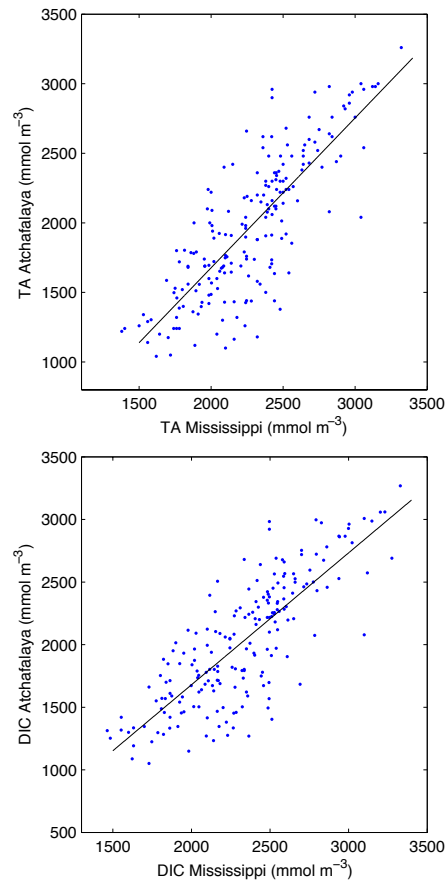


Figure S1. a) Scatterplot and adjusted linear regression for total alkalinity (TA) in the Mississippi river versus the Atchafalaya river; b) same as panel a but for dissolved inorganic carbon (DIC). The adjusted linear regressions are $TA_{AT} = 1.069 TA_{MS} - 456.4$ ($R^2 = 0.65$), and $DIC_{AT} = 1.045 TA_{MS} - 402.0$ ($R^2 = 0.64$).

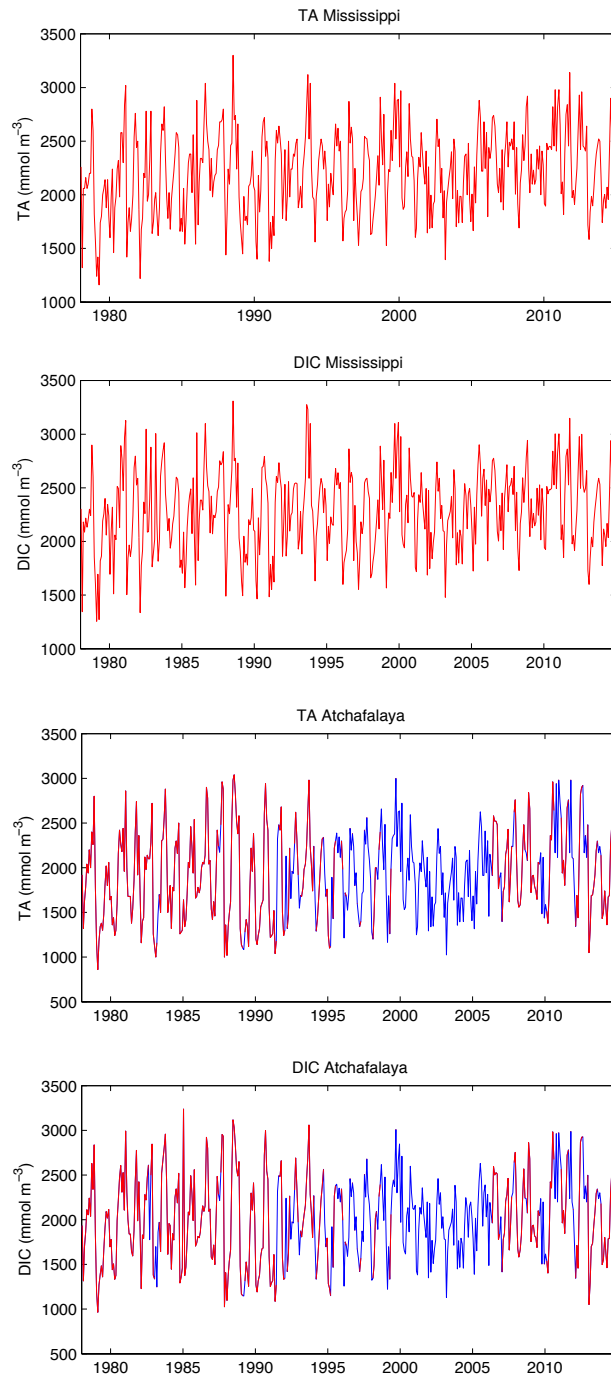


Figure S2. Time series of total alkalinity (TA) and dissolved inorganic carbon (DIC) in the Mississippi and Atchafalaya rivers. Red and blue lines in Atchafalaya river series are observed and interpolated values, respectively.

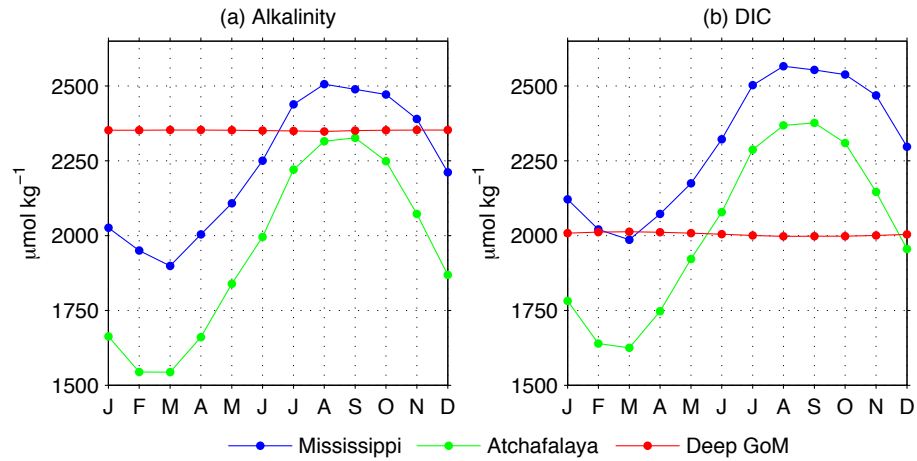


Figure S3. (a) Monthly mean alkalinity for the Mississippi and Atchafalaya rivers, as well as surface alkalinity over the deep Gulf of Mexico (deep GoM, derived from model's outputs), during 1981-2014. (b) As panel (a) but for dissolved inorganic carbon.

3. Atmospheric CO₂

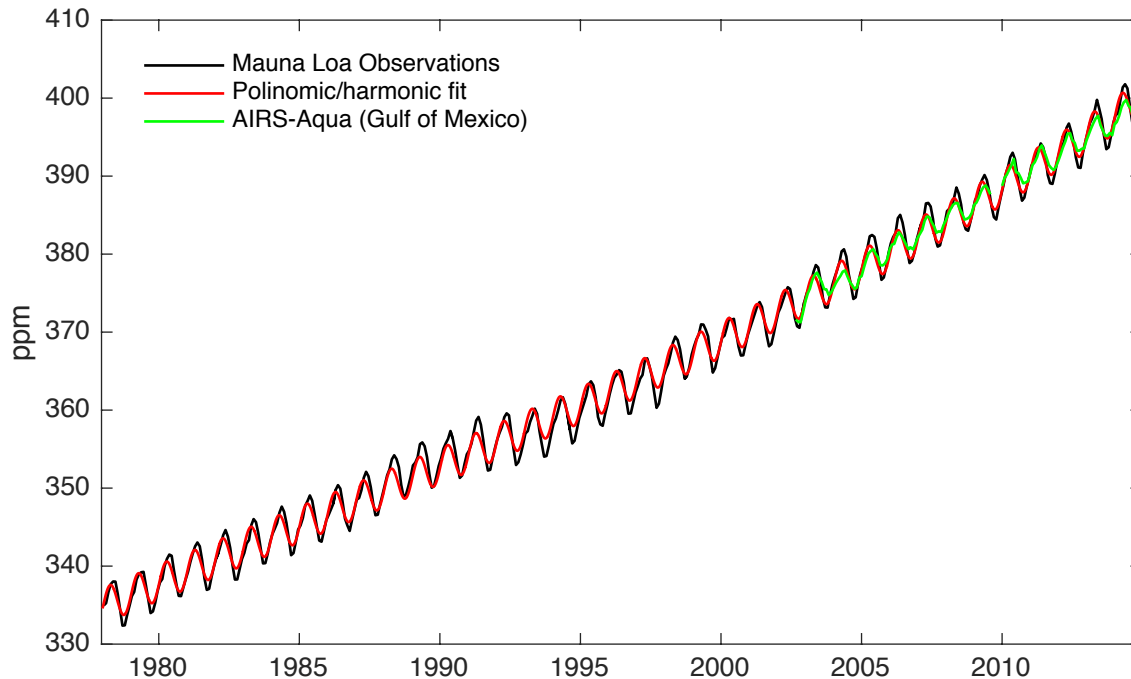


Figure S4. Monthly time series of atmospheric CO₂: Mauna Loa observations (black), polynomial-harmonic function adjusted to the Mauna Loa observations (red), and AIRS-Aqua CO₂ in the Gulf of Mexico (green).

The adjusted function used to prescribe atmospheric CO₂ (red line) is given by:

$$\begin{aligned} x\text{CO}_2(t) = & 334.8763 + 1.5127 \cdot t - 0.0055 \cdot t^2 + 0.0003 \cdot t^3 + \\ & 2.7656 \cdot \sin(2\pi t) - 0.9735 \cdot \cos(2\pi t) - 0.4750 \cdot \sin(2\pi t) + 0.6721 \cdot \cos(2\pi t) - \\ & 0.0755 \cdot \sin(2\pi t) + 0.0376 \cdot \cos(2\pi t) + 0.0505 \cdot \sin(2\pi t) - 0.0382 \cdot \cos(2\pi t) \end{aligned}$$

where $x\text{CO}_2$ is the mole fraction of CO₂ in ppm and t in years since January 1st 1978.

The adjusted values compare well with CO₂ observations from the Atmospheric Infrared Sounder (AIRS; <https://airs.jpl.nasa.gov/>; last access August 16th, 2018) spectrometer over the Gulf of Mexico during 2002-2014. Note that the AIRS series is column (stratospheric) CO₂. Although differences can be expected between surface and column CO₂, those differences are few ppm in the GoM.

4. Model and observed pCO₂ patterns across the Gulf of Mexico

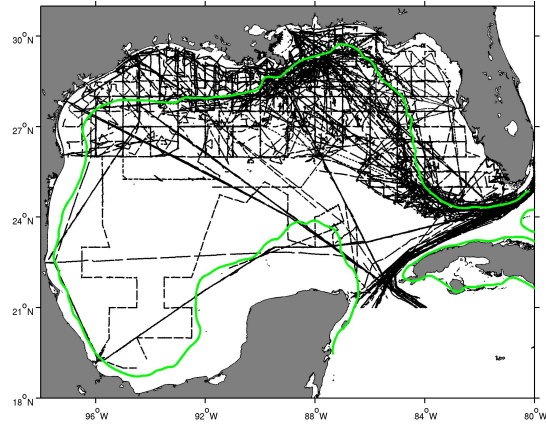


Figure S5. Tracks from ships of opportunity (SOOP) and research vessels that collected surface pCO₂ during 2005-2014. Green contour depicts the 200 m isobath.

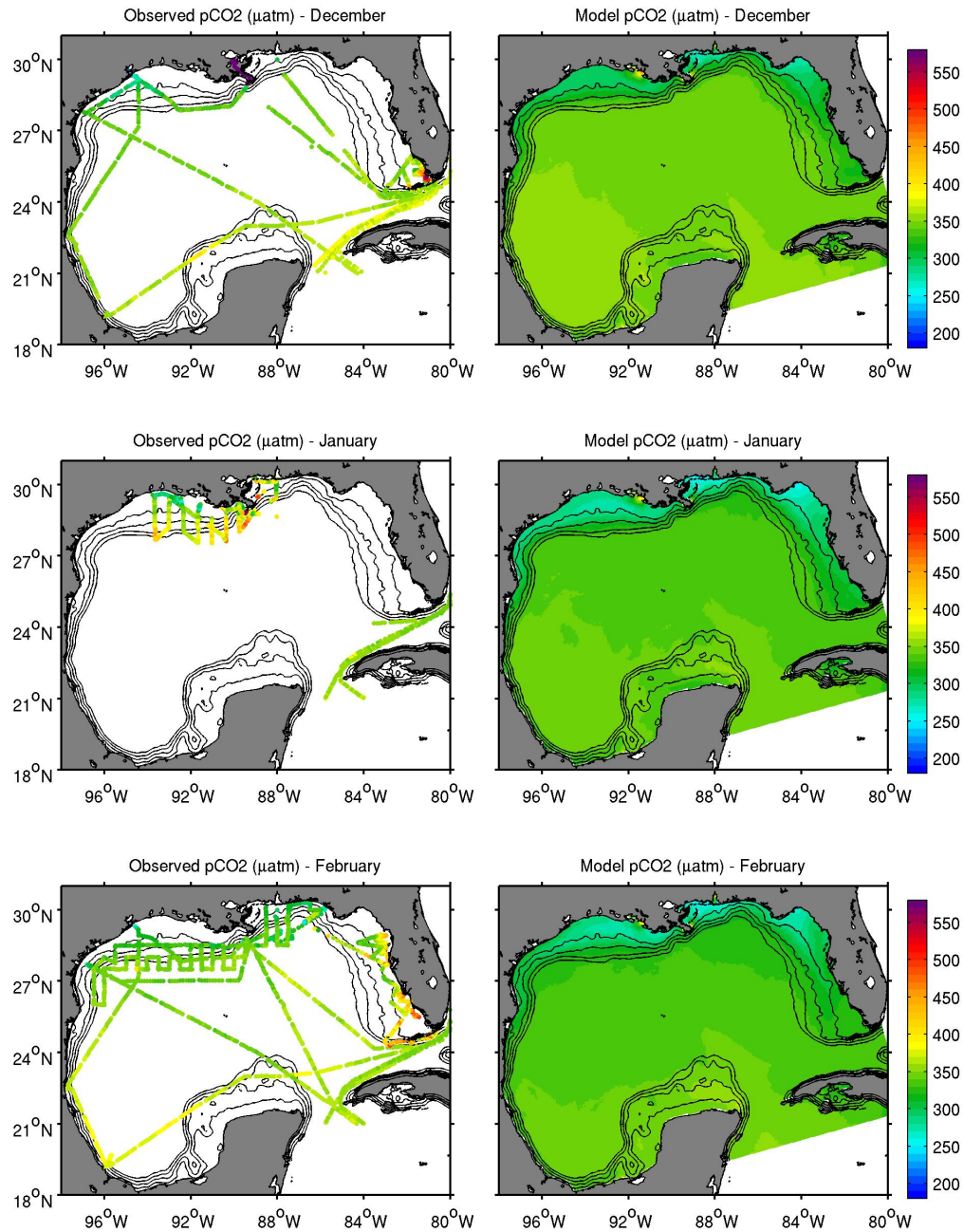


Figure S6. Monthly patterns of pCO₂: Observed pCO₂ (left panels) include measurements collected in research vessels and ships of opportunity during 2005-2014. Model pCO₂ (right panels) correspond to the monthly climatological mean from 2005-2014. Note that left panels in Fig. S6 display the raw pCO₂GoM_2018 measurements (not climatological averages), which can explain the smoother model's patterns when compared to the observations.

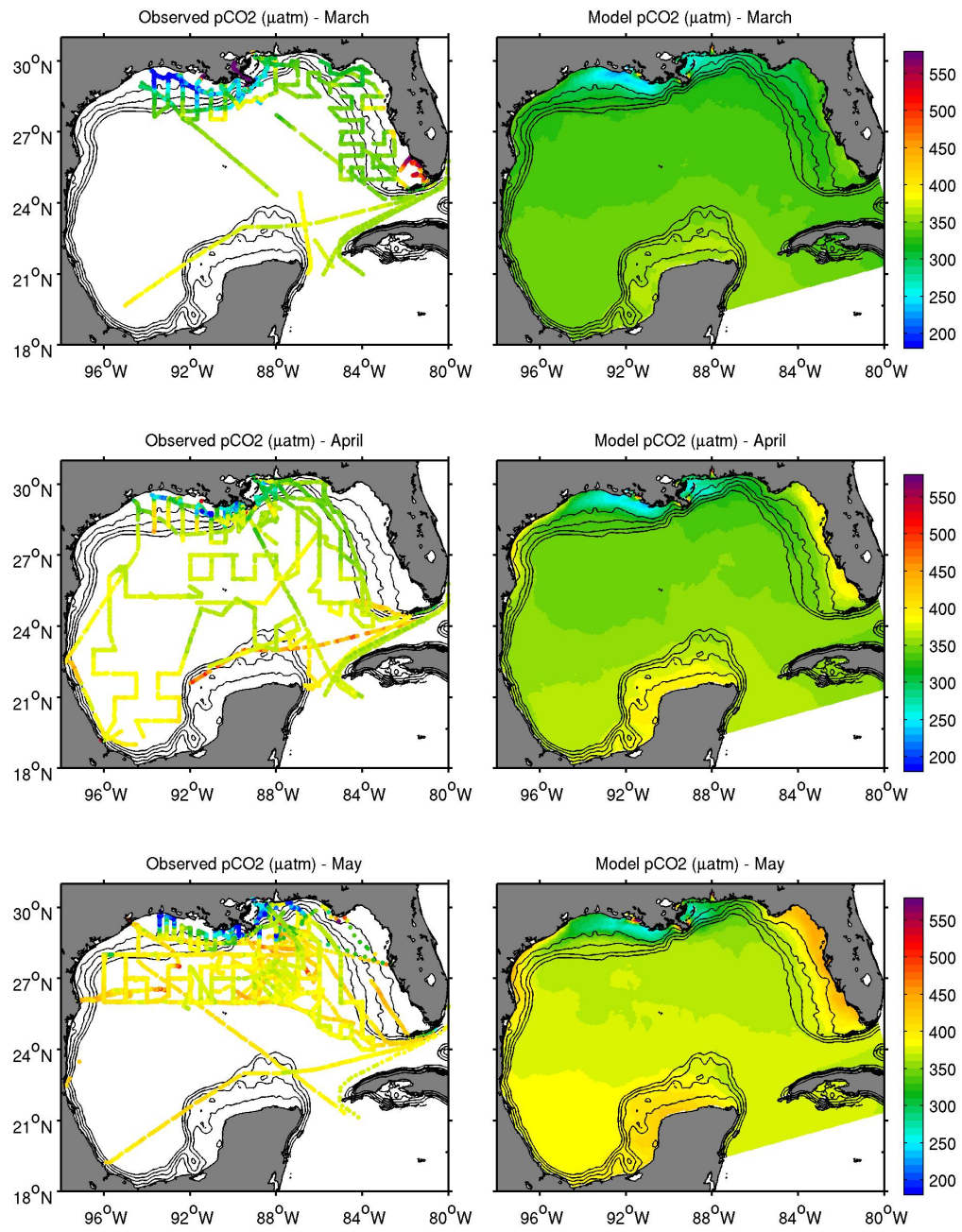


Figure S6. (Continuation).

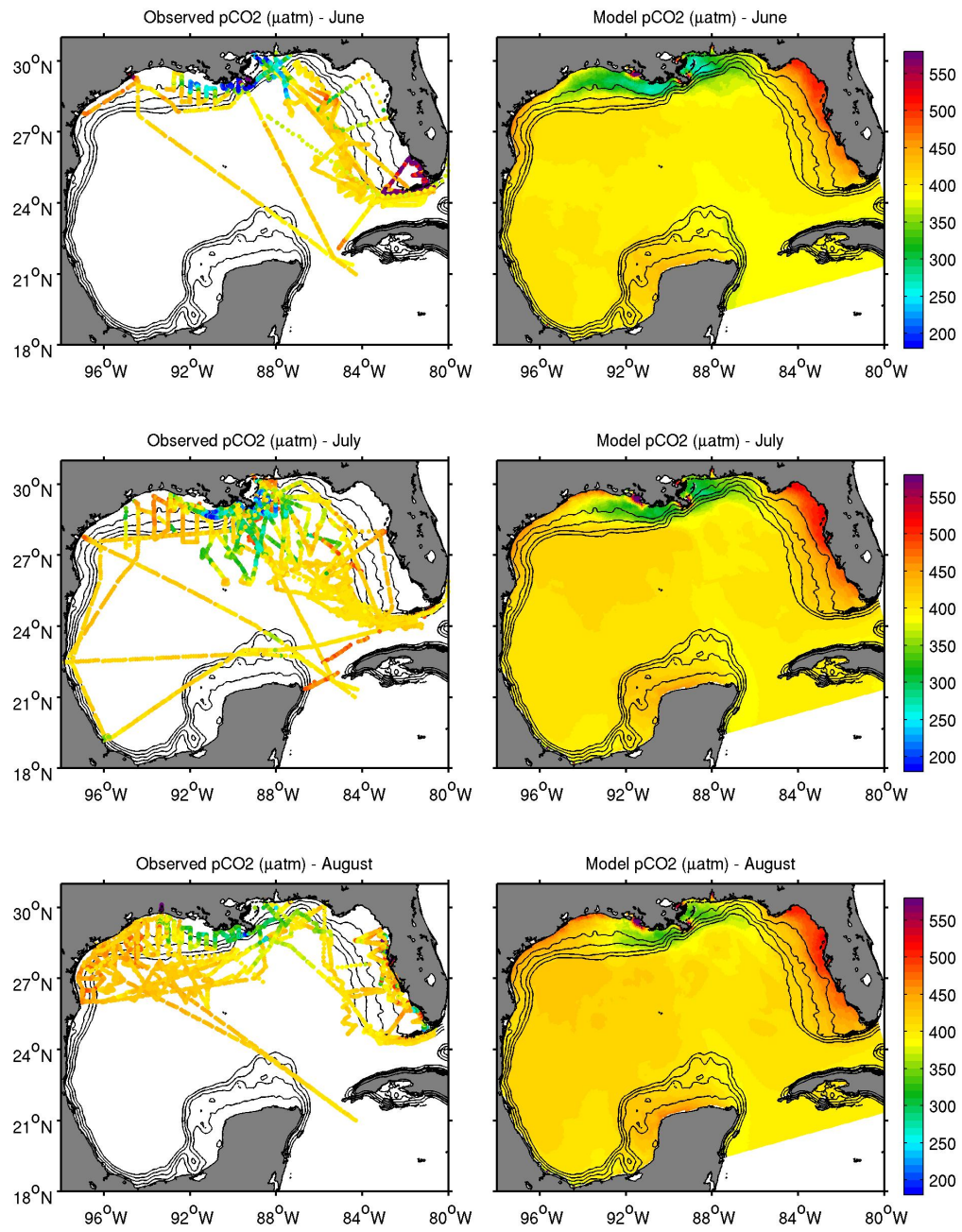


Figure S6. (Continuation).

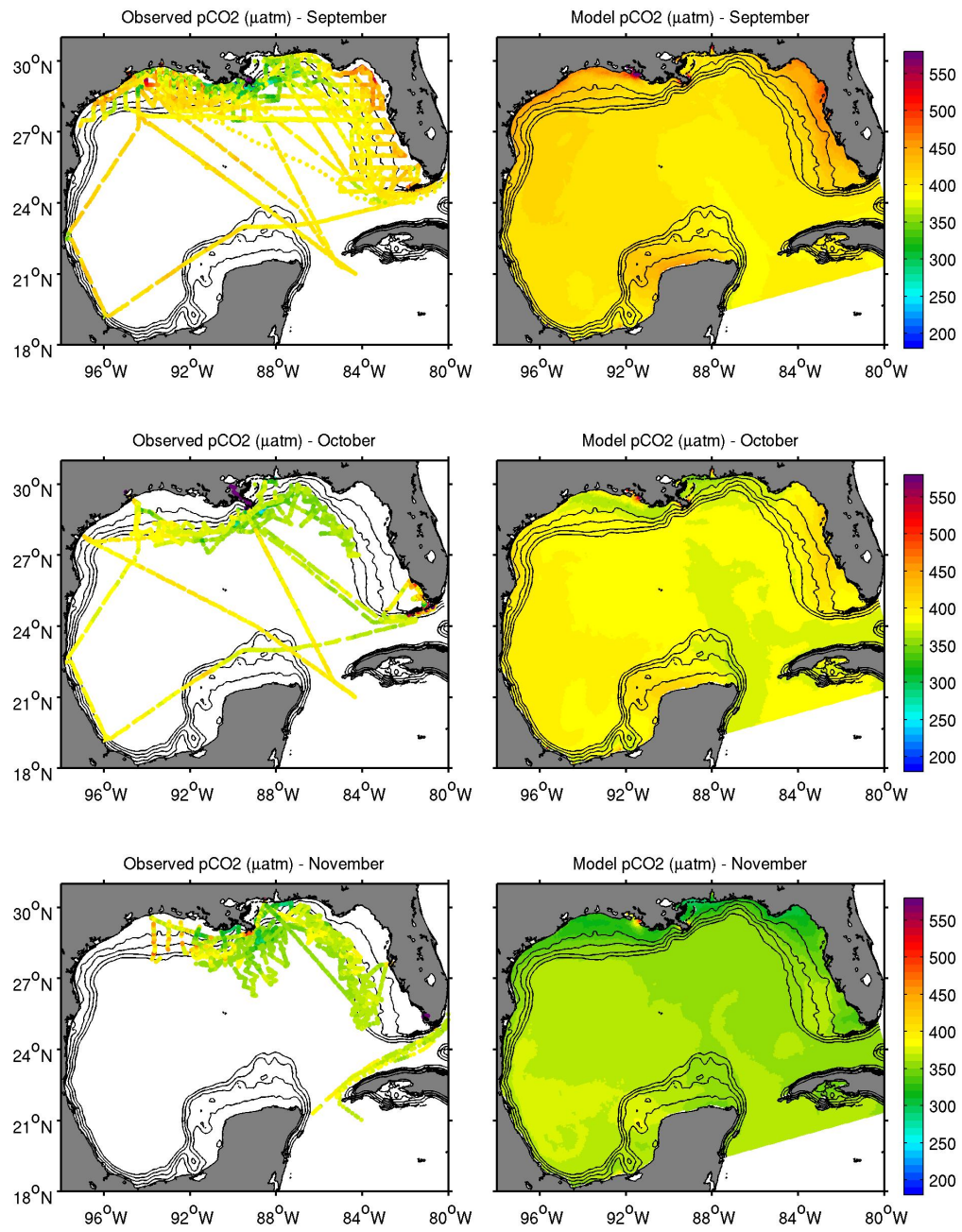


Figure S6. (Continuation).

5. Seasonal patterns for sea surface temperature

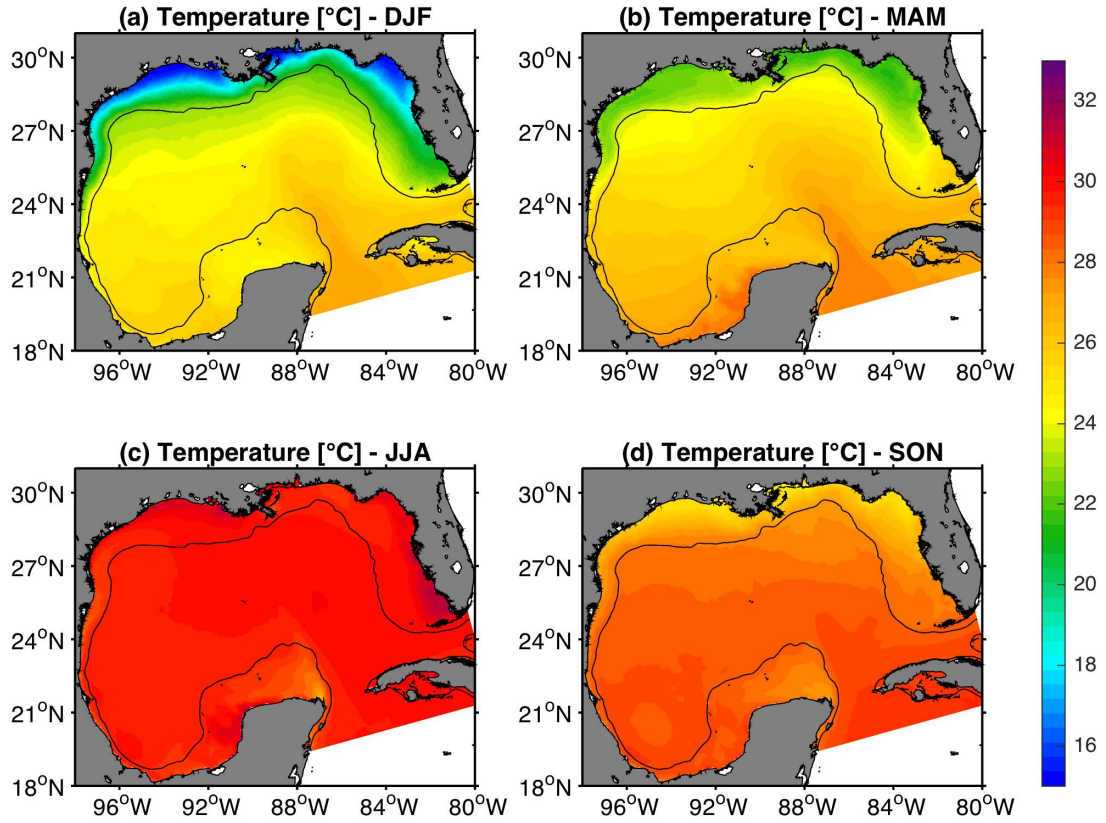


Figure S7. Mean model surface temperature in winter (DJF), spring (MAM), summer (JJA), and fall (SON) from 2005-2014. Black contour depicts the 200 m isobath.

6. Seasonal amplitude for surface aragonite saturation state and salinity

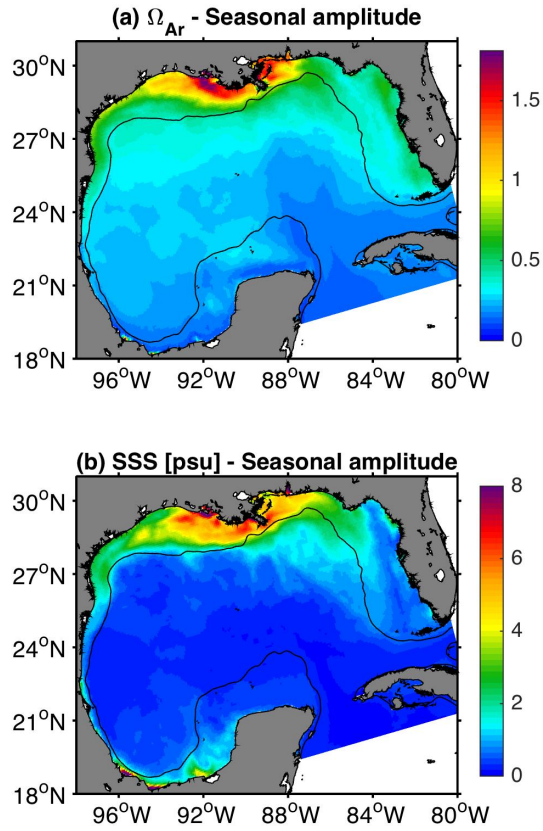


Figure S8. Seasonal amplitude patterns for surface aragonite saturation state and sea surface salinity from the model. Seasonal amplitude is defined as the difference between the maximum and minimum values from monthly average climatologies at each model grid point. Black contour depicts the 200 m isobath.

7. Seasonal patterns for surface salinity

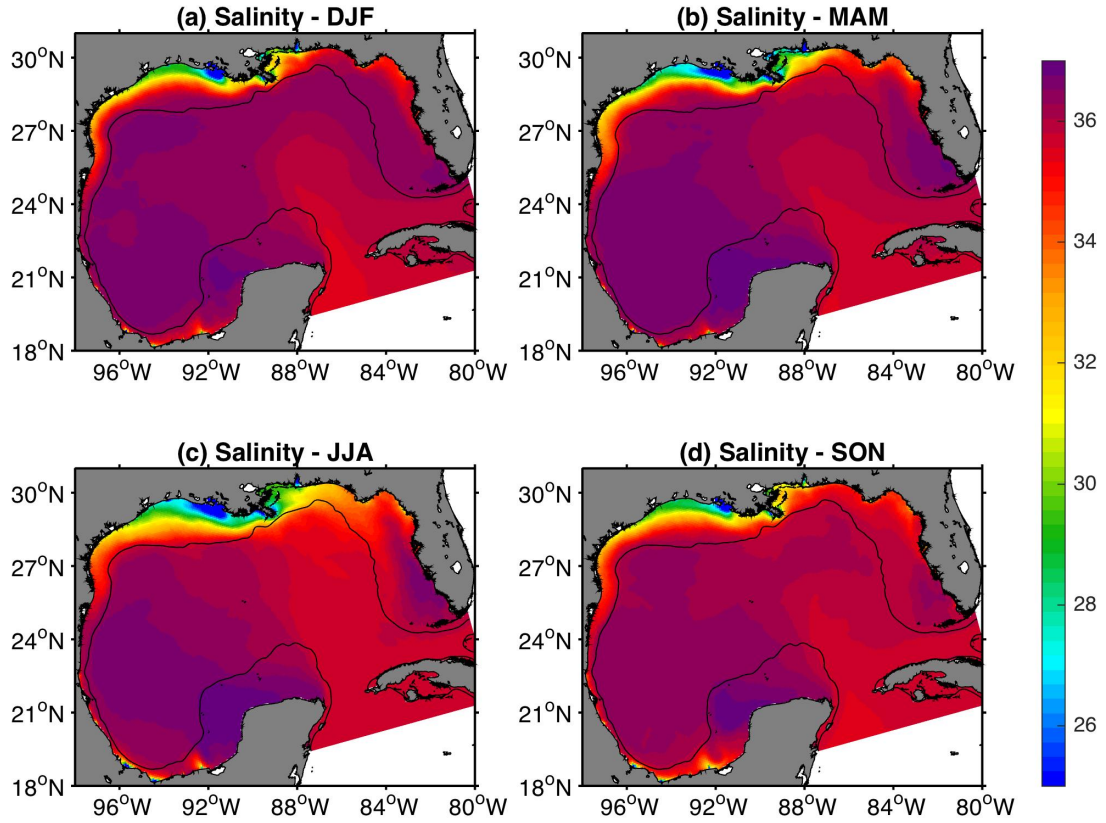


Figure S9. Mean model surface salinity in winter (DJF), spring (MAM), summer (JJA), and fall (SON) from 2005-2014. Black contour depicts the 200 m isobath.

8. Seasonal patterns for surface dissolved inorganic carbon

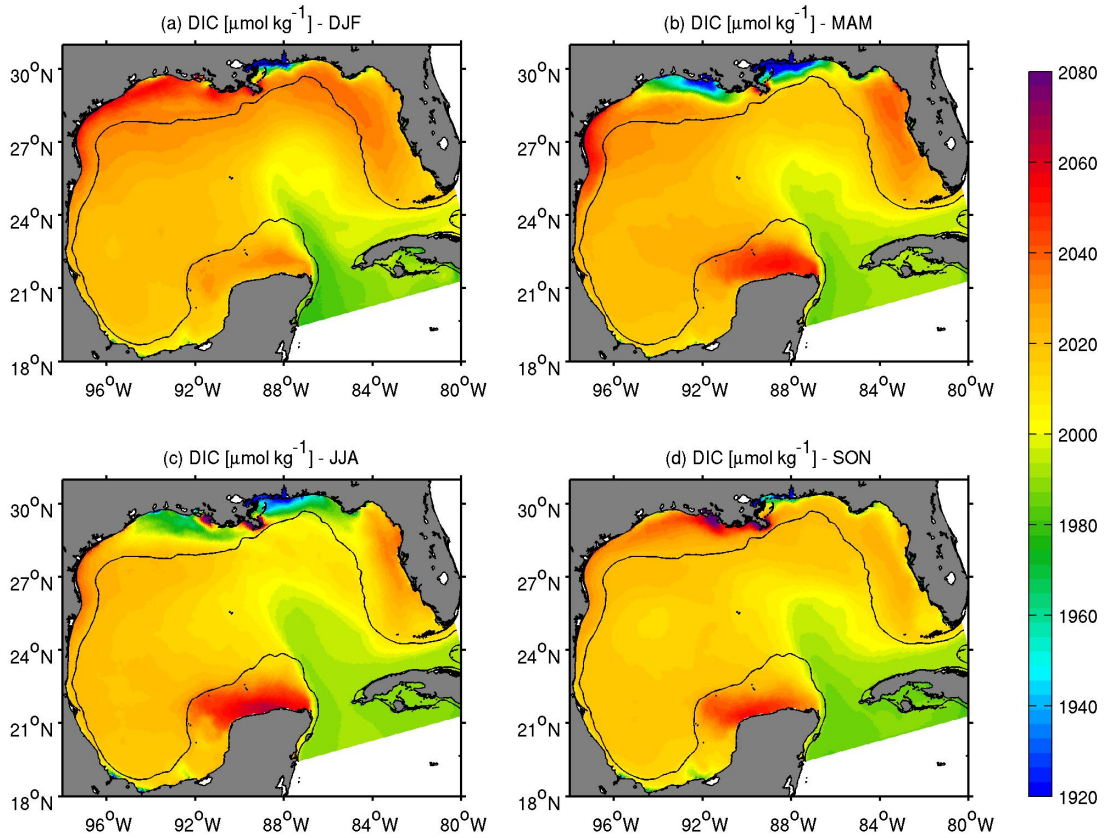


Figure S10. Mean model surface DIC in winter (DJF), spring (MAM), summer (JJA), and fall (SON) from 2005-2014. Black contour depicts the 200 m isobath.

9. Seasonal patterns for surface total alkalinity

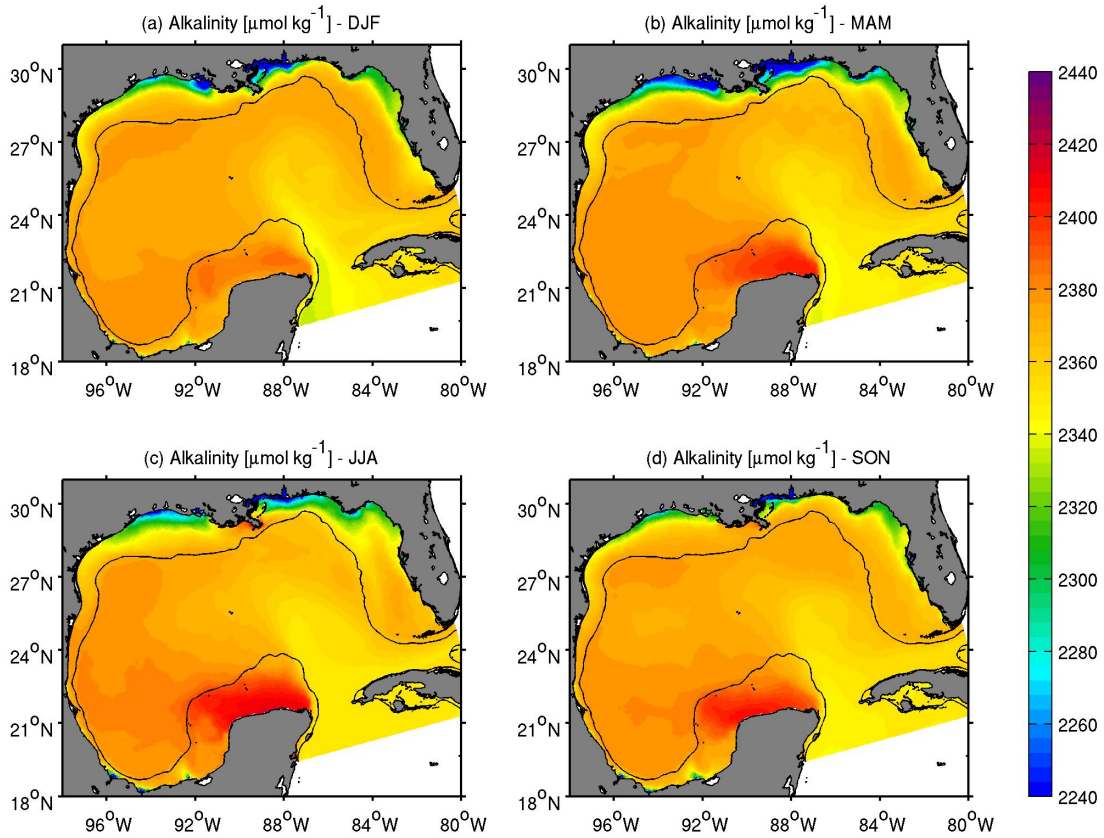


Figure S11. Mean model surface total alkalinity in winter (DJF), spring (MAM), summer (JJA), and fall (SON) from 2005-2014. Black contour depicts the 200 m isobath.

10. Zonal winds and carbon chemistry off northern Yucatan coast

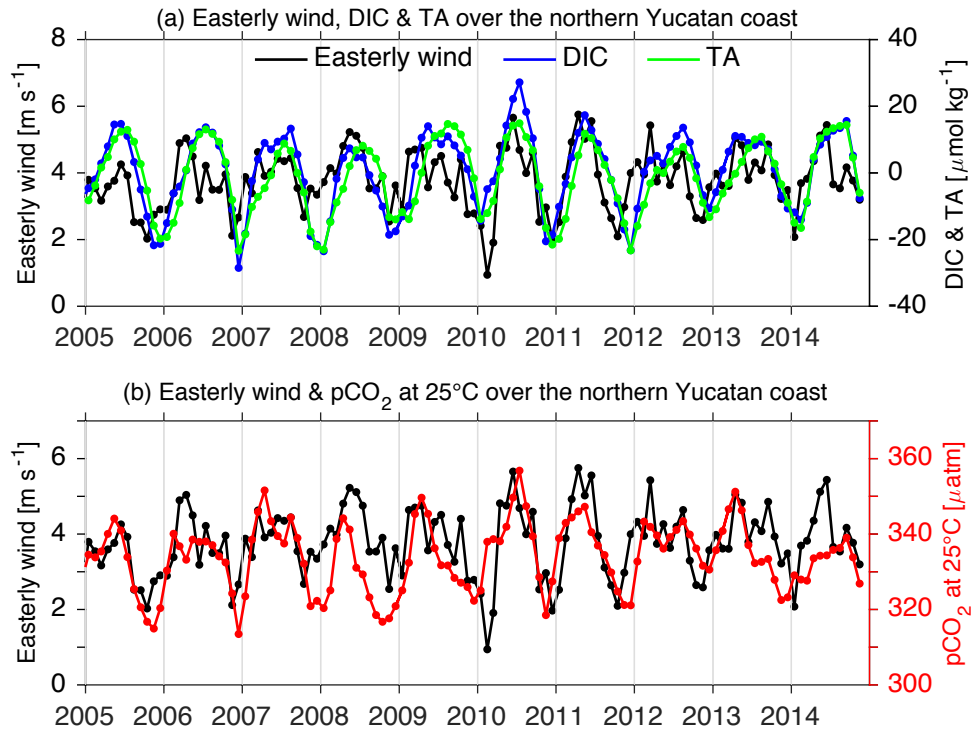


Figure S12. Detrended monthly time series of ERA-interim easterly winds (upwelling favorable for the northern Yucatan coast), model surface DIC and TA, and model surface pCO_2 (normalized at 25°C) over the northern Yucatan Peninsula margin. Note the long-term mean for the detrended DIC and TA series was removed ($2,025$ and $2,394 \mu\text{mol kg}^{-1}$, respectively).